Climate impacts of geoengineering in a delayed mitigation scenario

S. Tilmes[1], B. M. Sanderson[1], and B. O'Neill[1]

Simone Tilmes tilmes@ucar.edu

[1]National Center for Atmospheric

Research, Boulder CO, 80301

This article has been accepted for publication and undergone full peer review but has not been through the copyediting, typesetting, pagination and proofreading process, which may lead to differences between this version and the Version of Record. Please cite this article as doi: 10.1002/2016GL070122

Decarbonization in the immediate future is required to limit global mean temperature (GMT) increase to 2 degrees C relative to pre-industrial conditions, if geoengineering is not considered. Here we use the Community Earth System Model (CESM) to investigate climate outcomes if no mitigation is undertaken until GMT has reached 2 degree C. We find that late decarbonization (LD) in CESM without applying stratospheric sulfur injection (SSI) leads to a peak temperature increase of 3 degree C and GMT remains above 2 degrees for 160 years. An additional gradual increase and then decrease of SSI over this period reaching about 1.5 times the aerosol burden resulting from the Mt Pinatubo eruption in 1992 would limit the increase in GMT to 2.0 degrees for the specific pathway and model. SSI produces mean and extreme temperatures in CESM comparable to an early decarbonization pathway, but aridity is not mitigated to the same extent.

Keypoints:

- A scenario with aggressive decarbonization after unmitigated warming of 2 C has occurred leads to further warming of 1 C in CESM.
- In this late decarbonization scenario, stratospheric sulfur injection would be necessary for 160 years to limit warming to 2 C in CESM.
- Extremely warm temperatures but only some drying of land can be reduced in a late mitigation scenario including SRM in CESM.

1. Introduction

Global greenhouse gas emissions are increasing, roughly following a scenario with no mitigation policy that was described in the RCP8.5 scenario for CMIP5 [*Le Quéré et al.*, 2015; *Riahi et al.*, 2007]. In this scenario a global mean temperature (GMT)of 2 degrees C above pre-industrial is projected to be reached around 2035-2060, and GMT reaches around 4.5 $\pm$ 1.2 degrees C by the end of the century based multi-model results, leading to loss of summer Arctic sea-ice by the mid 21st century, increase of heat waves, flooding and droughts [*IPCC*, 2014]. Emissions mitigation could reduce these impacts [*Van Vuuren et al.*, 2007]. However, the recent Paris climate agreement [*United Nations Framework Convention for Climate Change*, 2015], to limit GMT change to below 2 degrees C, requires ambitious mitigation to be set into place in the next decade including rapid changes in the global energy infrastructure [*Stocker*, 2013; *Rogelj et al.*, 2015], not considering geoengineering options. The plausibility of such aggressive mitigation scenarios is controversial [*Rogelj et al.*, 2015; *Peters et al.*, 2013; *Geden*, 2015].

Stratospheric Sulfur Injection (SSI) has been suggested as a means of reducing global surface temperatures and associated impacts [*Crutzen*, 2006] instead of or in addition to decarbonization efforts [*Wigley*, 2006]. Decarbonization is defined here as the mitigation of positive emissions, as well as increasing net-negative emissions, e.g. carbon dioxide removal (CDR), itself a type of geoengineering [*Committee on Geoengineering Climate*, 2015]. Both geoengineering techniques have been assessed recently [*Committee on Geoengineering Climate*, 2015] and several studies have carried out simulations based on idealized scenarios to explore climate system processes determining responses to SSI [*Kravitz*

et al., 2011]. Arguably more realistic applications of SSI have been performed that are combined with mitigation to limit peak warming or reduce warming rates with simple climate models [*Keith and MacMartin*, 2015] or with global climate models using solar dimming to approximate the effect of stratospheric aerosols [*MacMartin et al.*, 2014a]. So far climate model studies have not explicitly simulated the effect of stratospheric aerosols to investigate climate impacts of SSI pathways that are aimed at limiting the GMT overshoot to a certain temperature goal. Our study limits CESM peak temperatures to 2 or 2.5 degrees C based on a newly designed late decarbonization pathway.

We investigate the role that SSI could play in achieving ambitious global temperature goals if mitigation action is delayed until the 2 degree target has been reached, which is the case around 2040 in CESM, when climate impacts are getting to the point that drastic changes may be seriously considered. Three scenarios are discussed: an aggressive late decarbonization (LD) pathway including strong mitigation and substantial negative CO_2 emissions, which leads to a temperature overshoot and eventual decline to a 2 degree target, and two scenarios that in addition to late decarbonization apply a time varying amount of SSI estimated to reduce peak warming to 2.5 C or to prevent any further warming beyond the 2 C level (SSI-2.5 and SSI-2.0 pathways).

In contrast to earlier studies by Wigley [2006], who only used a simple climate model, we use a state-of-the art climate model to investigate the outcome of specific pathways that include both decarbonization and SRM. We further estimate the amount of aerosol burden that would be required to reach the temperature goals specific to our model setup. Global and regional climate impacts are compared among these scenarios as well

as to an existing early decarbonization (ED) pathway (RCP2.6), which also limits GMT change to about 2 C. In addition to discussing precipitation changes, here we also apply a more comprehensive measure for aridity than used before in geoengineering studies. We further investigate the evolution of September Arctic sea-ice. Many other climate relevant diagnostics need to investigated in future studies.

We do not address questions of technical feasibility and additional potential side effects and risks associated with CDR and SSI. Those include impacts on the ozone layer, stratospheric chemistry [*Tilmes et al.*, 2008] and dynamics [*Aquila et al.*, 2014], implementation strategies [*MacMartin et al.*, 2014b], and other questions including costs, and political and ethical questions [*Committee on Geoengineering Climate*, 2015]. Our results provide a benchmark for exploring urgent scenarios for limiting climate change. Sensitivities of the results to specifics of the pathways including alternative overshoot scenarios with earlier or later starting dates and different decarbonization scenarios need to be investigated in future studies, that would vary maximum overshoot temperatures and required time and amount of SSI.

2. Experimental design

Three scenarios are designed using the Integrated Science Assessment Model (ISAM) simple climate model (see supplemental material). This model is calibrated using 15 free parameters to best emulate the global temperature evolution of Community Earth System Model (CESM) in the Coupled Model Intercomparison Project Phase 5 (CMIP5) Representation Concentration Pathway 8.6 (RCP8.5) experiment. The LD pathway is then constructed to follow RCP8.5 emissions for all forcing agents until 2040, when temper-

atures reached an increase of 2 degrees C compared to pre-industrial conditions. After 2040, total CO_2 emissions follow an idealized pathway using a functional form in which emissions peak in 2050 and then decline such that the maximum annual rate of decarbonization is equivalent to that seen in RCP3.4/SSP5 REMIND/MAGPIE simulation, which itself exhibits the highest rate of decarbonization in the SSP database (-1.2 Gt CO_2/yr/yr, database accessed November 2015). Emissions then decay to a constant negative emission "floor" of -18.5Gt CO_2/yr, a sustained level comparable to that assumed in the SSP5/RCP2.6 REMIND-MAGPIE simulation in the SSP database (Figure 1a). The other greenhouse gas emissions, including methane, nitrous oxide, and chlorofluorocarbons, follow a similar trend until their values reach RCP2.6 numbers (Figure S1, supplemental material). This produces an overshoot in atmospheric CO_2 concentrations peaking at 600 ppm and in ISAM-predicted surface temperatures with a peak of 3 C by the end of the 21st century.

We also use ISAM to estimate changes in global average forcing (relative to the LD pathway) necessary to limit warming to 2.5 or 2 C, as a basis for estimating the stratospheric sulfur loading to impose in CESM in the SSI-2.5 and SSI-2.0 simulations (Figure S2, supplemental material). The required annually evolving radiative forcing for CESM is then computed using the difference in shortwave top of atmosphere flux between the LD pathway and the respective SSI scenario. The SSI-2.5 scenario was designed in addition to the SSI-2.0 pathway to investigate a more moderate application of SSI to offset only part of the temperature increase beyond 2 degrees.

Global climate model simulations were performed using the same setup as used to produce the CESM Large Ensemble (LE) [*Kay et al.*, 2015]. This model is a fully coupled climate model, based on the CESM Version 1 model with Version 5 of the Community Atmosphere Model [*Hurrell et al.*, 2013].]. In this setup, the chemical composition of the atmosphere including ozone is prescribed. However, dynamical fields including temperature, winds, and water vapor, as well as radiation, respond to changes in the stratospheric aerosol burden. The LE consists of a 30-members of initial condition perturbation simulations from 1920 to 2100 all using the same external forcing (RCP8.5). Additionally, we employ results of one ensemble member of the RCP2.6 scenario.

New experiments were performed between 2040 and 2199 forced with emissions of anthropogenic aerosols that follow the RCP8.5 scenario, and the ISAM derived LD pathway concentration projections for greenhouse gases. For each simulation 2 ensemble members were produced. Prior to performing SSI-2.5 and SSI-2.0 simulations, the amount of stratospheric aerosol burden required to achieve the estimated time varying radiative forcing from the ISAM model was derived as follows. The radiative forcing reduction in CESM resulting from a prescribed stratospheric aerosol distribution was calculated using a double radiation call. We employed a prescribed distribution produced with a microphysical model [*Tilmes et al.*, 2015] driven by a continuous 8 Tg SO_2 per year tropical injection. The stratospheric aerosol burden in CESM was then varied over time by scaling it to achieve the required radiative forcing reaching up to 1.1 and 2.2 W/m^2 (as estimated with ISAM) and therefore to achieve the desired temperature evolution. Based on the scaling factor the injection amount was derived assuming that it is linearly related to

the aerosol burden, which is a good approximation for small injection amounts [*Niemeier et al.*, 2011]. Changes of the aerosol size distribution due to coagulation and deposition of aerosols with increasing injection amounts, as well as a potentially reduced climate response due to changes in the stratospheric composition in particular water vapor, has not been taken into account.

3. Results

Based on calculations using CESM, achieving the reduction in radiative forcing of 1.1 and 2.2. W/m^2 requires increasing the burden of stratospheric sulfur (S) by up to 3.5 Tg S for SSI-2.5 and up to 7 Tg S for SSI-2. to meet the 2.5 and 2.0 degree target, respectively (Figure 1, middle panel). The resulting burden is comparable to the effect of the largest volcanic eruptions in this century, which reached 5.5 Tg S (for Agung in 1963), and 4.5Tg S (for Mt Pinatubo in 1992), based on the CCMI stratospheric aerosol data set [*Eyring et al.*, 2013]. Corresponding maximum emissions of SO_2 necessary to produce these stratospheric aerosol burdens reach 8 million tons of SO_2 per year for SSI-2.5 and up to 17 million tons of SO_2 per year for SSI-2.0 (Figure 1, bottom panel). These estimates depend on the radiative response of the model that may vary by up to a factor of 2 between different model versions [*Neely et al.*, 2015]. Uncertainties also depend on the efficiency of the injection amount to produce a certain aerosol burden, which varies by injection strategy [*Niemeier et al.*, 2011; *English et al.*, 2012; *Pierce et al.*, 2010].

The CESM results follow the global mean surface temperature evolution predicted by ISAM (Figure 2a) despite the fact that a strong decarbonization pathway has not been performed before using CESM and additional climate feedbacks were not included in

ISAM. The simulated pathways show distinct global mean temperature evolutions within the first 20 years. The LD pathway leads to additional warming that peaks a full degree above the 2 C level reached in 2040 and persists for 160 years. SSI keeps temperatures from rising above 2.5 degrees C in SSI-2.5. A slight overcooling for the SSI-2.0 case (orange lines) to somewhat below the 2 degree target reflects the difficulty of precisely estimating injection amounts above about 10 Tg SO_2 injection per year between about 2060 and 2120. Nonetheless, in SSI-2.0 global temperatures over this time period are stabilized and similar to temperatures for the ED scenario, which are also slightly below 2 C.

Along with GMT changes, scenarios produce different outcomes for Northern Hemisphere sea-ice area (Figure 2b). The LD pathway cannot halt the sharply declining trend through 2040, driven by Arctic amplification of surface temperatures (Figure S3, supplemental material), leading to less than $0.2 \times 10^{12} m^2$ of sea-ice area by about 2060. SSI-2.5 also shows strongly reduced sea-ice area beyond 2040. Only SSI-2.0 keeps temperatures over the Arctic from increasing substantially and September sea-ice area around $1 \times 10^{12} m^2$ after 2040, similar to the result for the ED case. By the end of the 22nd century, as global average temperatures converge across scenarios, sea ice extent also converges to somewhat less than the value in 2040.

Global precipitation rates over land in the LD pathway strongly increase through about 2080 in accord with global temperatures (Figure 2c; see Figure S4, supplemental material, for global precipitation). The SSI-2.5 pathway halts the precipitation increase after about 2060, while SSI-2.0 leads to a decrease in precipitation below 2040 values until 2080. Global precipitation in SSI-2.0 is decreasing between 2040 and 2080, even though surface

temperatures are similar compared to the ED pathway, where precipitation is increasing until 2060. This illustrates that in SSI scenarios precipitation is more reduced than would be expected from their effect on GMT alone. These trends can be explained by changes in the surface energy budget (see supplementary material, Figure S5).

In SSI-2.0 and SSI-2.5 the high levels of greenhouse gases between 2040 and 2100 increase temperatures in the troposphere, while the artificial stratospheric aerosol burden reduces the net short wave (SW) radiation, and cools the surface. The surface cooling in SSI-2.0 to values similar to the ED pathway result in reduced latent heat flux and a slow-down of the hydrological cycle by the end of the 21st century [*Bala et al.*, 2010; *Schmidt et al.*, 2012; *Tilmes et al.*, 2013], while in SSI-2.5 latent heat flux is not reduced due to the slight increase in surface temperature relative to the ED pathway.

In contrast, the dominant effect in the ED pathway is the increase in the SW radiation due to reduced anthropogenic aerosols compared to present day. Those changes are balanced by an increase in latent heat fluxes and therefore result in increasing precipitation. Precipitation changes between different pathways can be expected to be significantly different between 2060 and 2120 based on only 2 ensemble members, assuming that each pathway describes has the same variability as the large ensemble simulation for RCP8.5, while differences are not significant before 2060 and after 2120. Between 2100 and 2200, the ramp-down of SSI and declining CO_2 concentration result in precipitation levels that converge over time to become similar across all pathways by 2200.

Pathways differ less in terms of aridity than they do for precipitation (Figure 2d). Aridity, measured using the Aridity Index (the ratio of precipitation to potential evapo-

transpiration, PET), is influenced not only by precipitation but also by changes in surface fluxes, surface temperatures, winds and humidity. The land surface generally becomes drier as warming proceeds [*Fu and Feng*, 2014]. PET across these scenarios tracks the global temperature response more closely than does precipitation (Figure S4, supplemental material). As a result, SSI-2.0 reduces drying less than it reduces precipitation consistent with mechanisms discussed in *Lin et al.* [2016]. The ED pathway is more effective in this regard, keeping aridity roughly constant at 2040 levels.

In terms of the regional impact, temperature effects differ significantly across regions in 2070–2100, when forcing levels strongly differ between the scenarios, while they converge across scenarios by 2170–2200 (Figure 3). In 2070–2100 the frequency of extreme summer heat (defined as monthly means above the current 95th percentile) in the LD pathway is significantly higher than in 2040, becoming 3-5 times more frequent than at present in North America, Western Europe, and India (additional regions and seasons are shown in Figures S7 to S9, supplemental material). The SSI scenarios reduce the frequency of extreme heat, with the SSI-2.0 and ED pathways both cutting the frequency about in half relative to the LD pathway.

Changes in extreme cold temperatures differ across regions and seasons (Figure 3, left panel). For North America, Europe, and West Africa, exceptionally cold months no longer occur in the LD pathway in 2070–2100, while in the SSI and ED pathways they are still very rare (reduction in frequency of 80% or more). In India and China (Figure S8, suppemental material) the reduction in frequency is smaller, ranging from 20-40%.

A more detailed investigation of regional precipitation and aridity distribution changes for different periods in comparison to present day shows for all pathways an increase in heavy precipitation occurrence and a reduction in medium precipitation for most regions besides for West Africa, and some increase in very low precipitation for Western Europe and North America in summer (Figure S10, supplemental material). SSI does not significantly suppress these changes in heavy precipitation events, and therefore would be unlikely to significantly change the occurrence of flooding in most regions compared to the LD pathway.

The distribution of wet and dry land, defined as having an aridity index above or below 0.65, respectively, shifts significantly toward dry land between 1986–2005 and 2070–2100 in all regions for RCP8.5, the LD pathway, and the SSI scenarios, with significantly smaller change for the ED pathway (Figure 4). In all scenarios there is little change in aridity by the end of the 22nd century compared to present day. The discussed regional changes may be model dependent and multi-model comparisons are required to identify more robust regional changes in particular in the hydrological cycle.

4. Conclusions

In summary, if climate actions are delayed until 2 degrees of warming has been reached, rapid mitigation would likely need to be combined with significant geoengineering efforts including CDR and SSI to maintain temperatures below 2 degrees above pre-industrial. An additional 2.5 degree SSI pathway has been investigated to explore the characteristics of a less strong SSI pathway. Based on CESM simulations, the artificial injection of up to 18 Tg SO_2 for SSI 2.0 and 8 Tg SO_2 for SSI 2.5 into the upper atmosphere can

constrain temperature increase to below 2 C and 2.5 C respectively. SSI 2.0 would produce changes in temperature extremes and September sea-ice comparable to those in an early action pathway (ED) without SSI. The increase in precipitation induced by increasing greenhouse gas and decreasing tropospheric aerosol concentrations in an LD pathway would be substantially reduced to values below those that exist in 2040 before SSI begins. The 2.5C scenario would stabilize global precipitation values in the 21st century but extreme temperatures and Arctic sea-ice are not reduced as effectively. Both pathways would do less to reduce increases in aridity compared to the ED pathway.

Results are likely to be strongly model and pathway dependent, including estimated injection amounts, global and especially regional temperature and precipitation changes. Further investigations of pathways discussed in this paper, for example as a part of the Geoengineering Model Intercomparison Projects (GeoMIP), would facilitate a more in-depth understanding of the potential impacts of SSI in a mixed mitigation/geoengineering scenario. Furthermore, the plausibility of the pathways investigated here is uncertain given that neither CDR technologies to actively remove large amounts of CO_2 from the atmosphere nor solar radiation management technologies have been developed yet that could be employed at the required scales.

Acknowledgments. We thank Yangyang Xu and John Fasullo for helpful discussions on the paper. The CESM project is supported by the National Science Foundation and the Office of Science (BER) of the U. S. Department of Energy. The National Center for Atmospheric Research is funded by the National Science Foundation.

References

Aquila, V., C. I. Garfinkel, P. Newman, L. Oman, and D. Waugh (2014), Modifications of the quasi-biennial oscillation by a geoengineering perturbation of the stratospheric aerosol layer, *Geophysical Research Letters*, *41*(5), 1738–1744, doi: 10.1002/2013GL058818.

Bala, G., K. Caldeira, R. Nemani, L. Cao, G. Ban-Weiss, and H.-J. Shin (2010), Albedo enhancement of marine clouds to counteract global warming: impacts on the hydrological cycle, *Climate Dynamics*, *37*(5-6), 915–931, doi:10.1007/s00382-010-0868-1.

Committee on Geoengineering Climate (2015), *Climate Intervention:: Reflecting Sunlight to Cool Earth, and Carbon Dioxide Removal and Reliable Sequestration*, National Academies Press.

Crutzen, P. J. (2006), Albedo enhancements by stratospheric sulfur injections: A contribution to resolve a policy dilemma? An Editorial Essay, *Clim. Change*, *77*, 211–219.

English, J. M., O. B. Toon, and M. J. Mills (2012), Microphysical simulations of sulfur burdens from stratospheric sulfur geoengineering, *Atmospheric Chemistry and Physics*, *12*(10), 4775–4793, doi:10.5194/acp-12-4775-2012.

Eyring, V., J.-F. Lamarque, and P. Hess (2013), Overview of IGAC/SPARC Chemistry-Climate Model Initiative (CCMI) Community Simulations in Support of Upcoming Ozone and Climate Assessments, *Tech. rep.*, doi:SPARC Newsletter No. 40, p. 48-66, 2013.

Fu, Q., and S. Feng (2014), Responses of terrestrial aridity to global warming, *Journal of Geophysical Research: Atmospheres*, *119*(13), 7863–7875, doi:10.1002/2014JD021608.

Geden, O. (2015), Climate advisers must maintain integrity, *Nature*, *521*(Comment), 27–28, doi:10.1038/521027a.

Hurrell, J. W., H. M. M., P. R. Gent, S. Ghan, J. E. Kay, P. H. Kushner, J.-F. Lamarque, W. G. Large, D. Lawrence, L. K., W. H. Lipscomb, C. L. M, N. Manhowald, D. R. Marsh, R. B. Beale, P. Rasch, S. Vavrus, M. Verteinstein, D. Bader, W. D. Collins, J. J. Hack, J. Kiehl, and S. Marshall (2013), A Framework for Collaborative Research, *B. Am. Meteorol. Soc.*, *94*(November 2012), 1339–1360, doi:10.1175. BAMS-D-12-00121.1.

IPCC (2014), *Climate Change 2014-Impacts, Adaptation and Vulnerability: Regional Aspects*, Cambridge University Press.

Kay, J. E., C. Deser, A. Phillips, A. Mai, C. Hannay, G. Strand, J. M. Arblaster, S. C. Bates, G. Danabasoglu, J. Edwards, M. Holland, P. Kushner, J. F. Lamarque, D. Lawrence, K. Lindsay, A. Middleton, E. Munoz, R. Neale, K. Oleson, L. Polvani, and M. Vertenstein (2015), The community earth system model (CESM) large ensemble project : A community resource for studying climate change in the presence of internal climate variability, *Bulletin of the American Meteorological Society*, *96*(8), 1333–1349, doi:10.1175/BAMS-D-13-00255.1.

Keith, D. W., and D. G. MacMartin (2015), A temporary, moderate and responsive scenario for solar geoengineering, *Nature Climate Change*, *5*(3), 201–206, doi:10.1038/nclimate2493.

Kravitz, B., A. Robock, O. Boucher, H. Schmidt, K. E. Taylor, G. Stenchikov, and M. Schulz (2011), The Geoengineering Model Intercomparison Project (GeoMIP), *Atmospheric Science Letters*, *12*(2), 162–167, doi:10.1002/asl.316.

Le Quéré, C., R. Moriarty, R. M. Andrew, G. P. Peters, P. Ciais, P. Friedlingstein, S. D. Jones, S. Sitch, P. Tans, A. Arneth, T. A. Boden, L. Bopp, Y. Bozec, J. G. Canadell, L. P. Chini, F. Chevallier, C. E. Cosca, I. Harris, M. Hoppema, R. A. Houghton, J. I. House, A. K. Jain, T. Johannessen, E. Kato, R. F. Keeling, V. Kitidis, K. Klein Goldewijk, C. Koven, C. S. Landa, P. Landschützer, A. Lenton, I. D. Lima, G. Marland, J. T. Mathis, N. Metzl, Y. Nojiri, A. Olsen, T. Ono, S. Peng, W. Peters, B. Pfeil, B. Poulter, M. R. Raupach, P. Regnier, C. Rödenbeck, S. Saito, J. E. Salisbury, U. Schuster, J. Schwinger, R. Séférian, J. Segschneider, T. Steinhoff, B. D. Stocker, A. J. Sutton, T. Takahashi, B. Tilbrook, G. R. Van Der Werf, N. Viovy, Y. P. Wang, R. Wanninkhof, A. Wiltshire, and N. Zeng (2015), Global carbon budget 2014, *Earth System Science Data*, *7*(1), 47–85, doi:10.5194/essd-7-47-2015.

Lin, L., A. Gettelman, Q. Fu, and Y. Xu (2016), Simulated differences in 21st century aridity due to different scenarios of greenhouse gases and aerosols, *Climatic Change*, doi:10.1007/s10584-016-1615-3.

MacMartin, D. G., K. Caldeira, and D. W. Keith (2014a), Solar geoengineering to limit the rate of temperature change., *Philosophical Transactions of the Royal Society A*, *372*, 20140,134, doi:10.1098/rsta.2014.0134.

MacMartin, D. G., B. Kravitz, D. W. Keith, and A. Jarvis (2014b), Dynamics of the coupled human-climate system resulting from closed-loop control of solar geoengineering, *Climate Dynamics*, *43*(1-2), 243–258, doi:10.1007/s00382-013-1822-9.

Neely, R. R., A. Conley, F. Vitt, and J. F. Lamarque (2015), A Consistent Prescription of Stratospheric Aerosol for Both Radiation and Chemistry in the Community Earth

System Model (CESM1), *Geoscientific Model Development Discussions*, *8*(12), 10,711–10,734, doi:10.5194/gmdd-8-10711-2015.

Niemeier, U., H. Schmidt, and C. Timmreck (2011), The dependency of geoengineered sulfate aerosol on the emission strategy, *Atmospheric Science Letters*, *12*(2), 189–194, doi:10.1002/asl.304.

Peters, G. P., R. M. Andrew, T. Boden, J. G. Canadell, P. Ciais, C. L. Quéré, G. Marland, M. R. Raupach, and C. Wilson (2013), The challenge to keep global warming below 2 C, *Nature Climate Change*, *3*(1), 2–4, doi:10.1038/nclimate1783.

Pierce, J. R., D. K. Weisenstein, P. Heckendorn, T. Peter, and D. W. Keith (2010), Efficient formation of stratospheric aerosol for climate engineering by emission of condensible vapor from aircraft, *Geophysical Research Letters*, *37*(18), n/a–n/a, doi:10.1029/2010GL043975.

Riahi, K., A. Grübler, and N. Nakicenovic (2007), Scenarios of long-term socio-economic and environmental development under climate stabilization, *Technological Forecasting and Social Change*, *74*(7), 887–935, doi:10.1016/j.techfore.2006.05.026.

Rogelj, J., G. Luderer, R. C. Pietzcker, E. Kriegler, M. Schaeffer, V. Krey, and K. Riahi (2015), Energy system transformations for limiting end-of-century warming to below 1.5 [deg]C, *Nature Clim. Change*, *5*(6), 519–527.

Schmidt, H., K. Alterskjær, D. Bou Karam, O. Boucher, A. Jones, J. E. Kristjánsson, U. Niemeier, M. Schulz, A. Aaheim, F. Benduhn, M. Lawrence, and C. Timmreck (2012), Solar irradiance reduction to counteract radiative forcing from a quadrupling of CO2: climate responses simulated by four earth system models, *Earth System Dynam-*

ics, *3*(1), 63–78, doi:10.5194/esd-3-63-2012.

Stocker, T. F. (2013), The closing door of climate targets., *Science*, *339*(6117), 280–2, doi:10.1126/science.1232468.

Tilmes, S., R. Müller, and R. Salawitch (2008), The sensitivity of polar ozone depletion to proposed geoengineering schemes., *Science*, *320*(5880), 1201–1204, doi:10.1126/science.1153966.

Tilmes, S., J. Fasullo, J.-F. Lamarque, D. R. Marsh, M. Mills, K. Alterskjaer, H. Muri, J. E. Kristjánsson, O. Boucher, M. Schulz, J. N. S. Cole, C. L. Curry, A. Jones, J. Haywood, P. J. Irvine, D. Ji, J. C. Moore, D. B. Karam, B. Kravitz, P. J. Rasch, B. Singh, J.-H. Yoon, U. Niemeier, H. Schmidt, A. Robock, S. Yang, and S. Watanabe (2013), The hydrological impact of geoengineering in the Geoengineering Model Intercomparison Project (GeoMIP), *Journal of Geophysical Research: Atmospheres*, *118*(19), 11,036–11,058, doi:10.1002/jgrd.50868.

Tilmes, S., M. J. Mills, U. Niemeier, H. Schmidt, A. Robock, B. Kravitz, J.-F. Lamarque, G. Pitari, and J. M. English (2015), A new Geoengineering Model Intercomparison Project (GeoMIP) experiment designed for climate and chemistry models, *Geoscientific Model Development*, *8*(1), 43–49, doi:10.5194/gmd-8-43-2015.

United Nations Framework Convention for Climate Change (2015), Synthesis report on the aggregate effect of the intended nationally determined contributions, *FCCC/CP*(2015/7), 1–66.

Van Vuuren, D. P., M. G. J. Den Elzen, P. L. Lucas, B. Eickhout, B. J. Strengers, B. Van Ruijven, S. Wonink, and R. Van Houdt (2007), Stabilizing greenhouse gas

concentrations at low levels: An assessment of reduction strategies and costs, *Climatic Change*, *81*(2), 119–159, doi:10.1007/s10584-006-9172-9.

Wigley, T. M. (2006), A combined mitigation/geoengineering approach to climate stabilization, *Science*, *314*, 452–454.

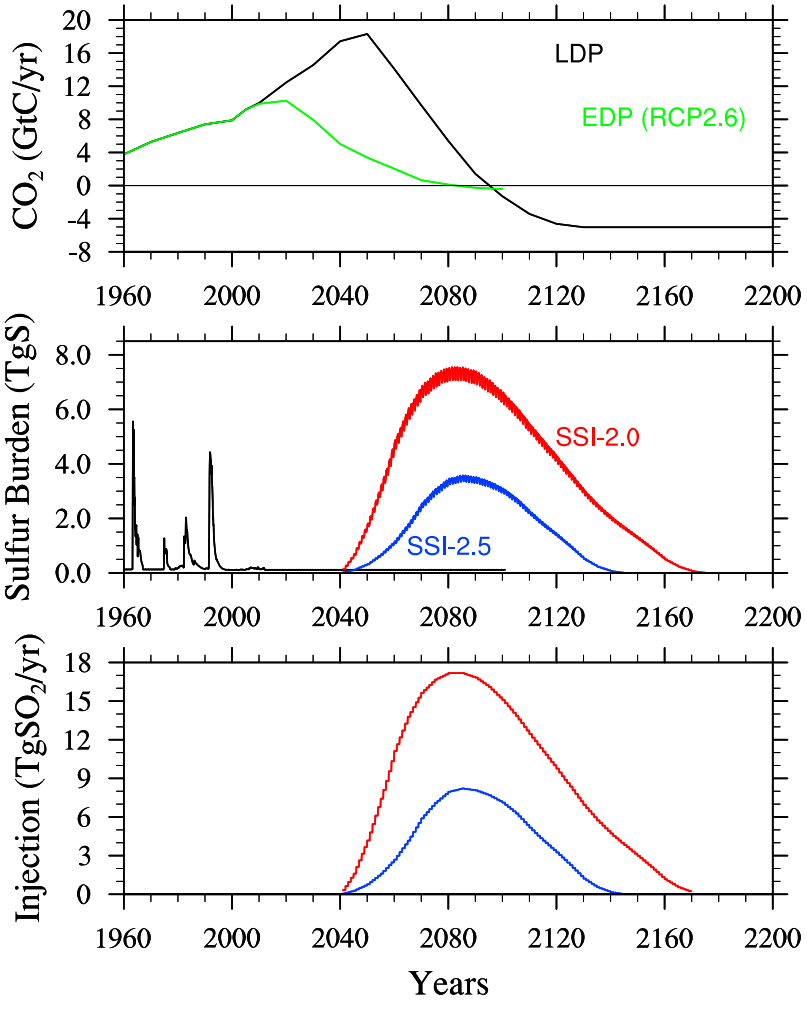

Figure 1. Time evolution of CO_2 emissions, sulfur forcings and injection amount. Top panel: ISAM derived CO_2 emission evolution for the LD pathway, SSI2.5 and SSI2.0, black, and the ED pathway (RCP2.6), green. Middle panel: Stratospheric sulfur burden in Tg S (in form of H_2SO_4) per year, based on the prescribed aerosol data set for the Chemistry Climate Model Initiative [*Eyring et al.*, 2013] (black), SSI-2.5 (blue) and SSI-2.0 (red), Bottom panel: Estimated injection in $TgSO_2$/yr for SSI-2.5 (blue) and SSI-2.0 (red).

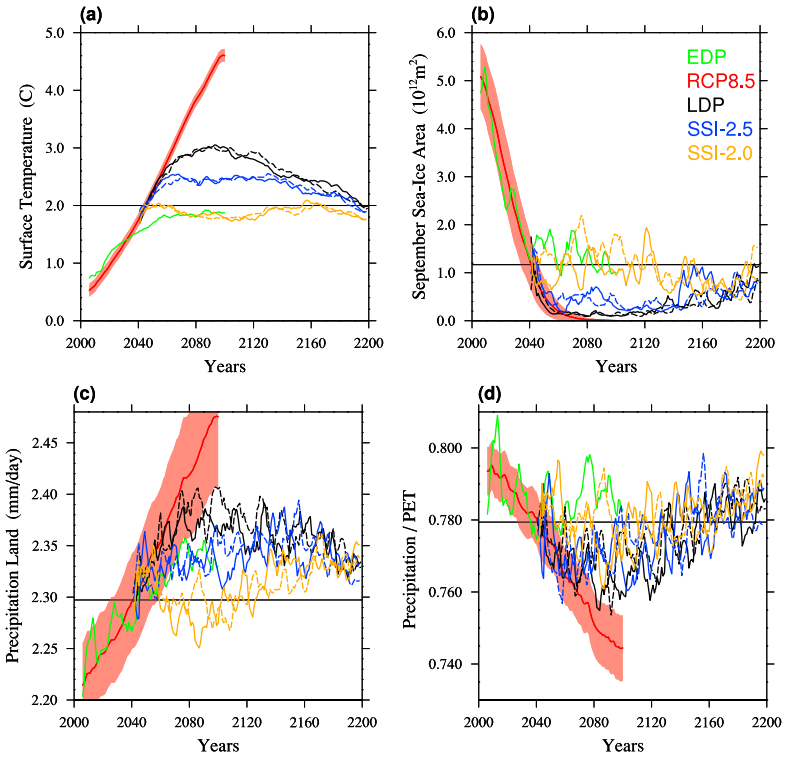

Figure 2. Time evolution of global and annual averages. Surface temperature (a), Northern Hemisphere September sea-ice area (b), precipitation over land (c), and the aridity index (precipitation/Potential Evapotranspiration (PET)) (d), for different scenarios. A ten year running mean was applied. Different colors identify different experiments and ensemble members (see legend). For RCP8.5, shaded areas indicate the standard deviation of results including all 30 members of the large ensemble.

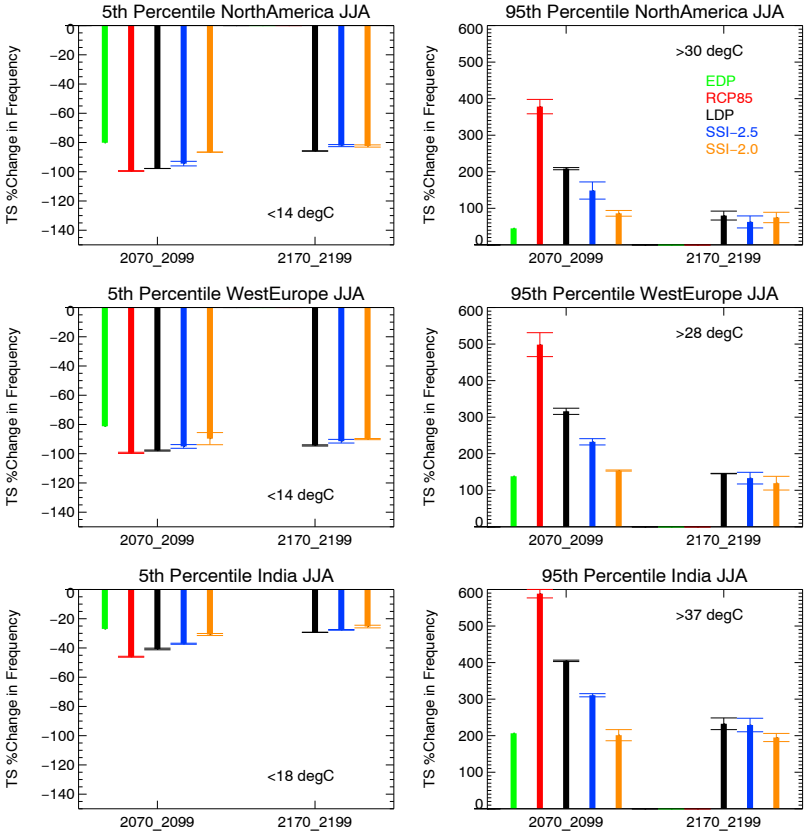

Figure 3. Regional change in extreme temperature occurrence in summer. Relative change in the frequency of summer months, June-July-August (JJA), with extreme cold (left panels) and extreme heat (right panels) for 2070–2099 and 2170–2199 compared to 1986–2005, defined as monthly mean surface temperature below the 5th or above the 95th percentile of the probability distribution function (PDF) based on 1986–2005, for different regions as defined in Figure 6S, supplemental material: North America (top), Western Europe (middle), and India (bottom). The value of the 5th and 95th percentile is illustrated in each panel. Error bars indicate the standard deviation of available ensemble members for each pathway.

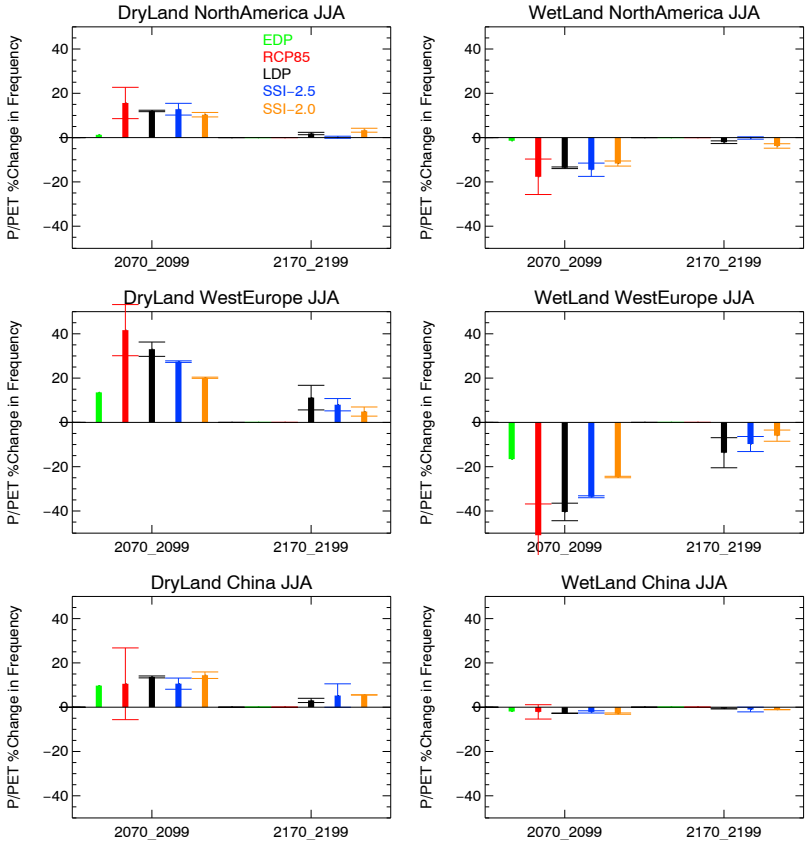

Figure 4. Regional change in dry and wet land occurrence in summer. Relative change in the frequency of the aridity index (P/PET) for summer months over dry lands (left panels) and wet lands (right panels), defined as monthly mean aridity below or above 0.65 of the Aridity Index distribution for 2070–2099 and 2170–2199 compared to 1986–2005, for different regions as defined in Figure 6S, supplemental material: North America (top), Western Europe (middle), and China (bottom). Error bars indicate the standard deviation of available ensemble members for each pathway.